

Supplementary Materials

**Unveiling the synergistic effect of two-dimensional
heterostructure NiFeP@FeOOH as stable electrocatalyst for
oxygen evolution reaction**

1. Material characterizations

The morphology and structure of NiFeP@FeOOH/NF and its precursor were studied using a field emission scanning electron microscope (FESEM, JEOL JSM-6700F, Japan), a high-resolution transmission electron microscope (HRTEM, JEOL-2100Plus, Japan), and X-ray diffraction (XRD, Rigaku Ultima IV, Japan) with an energy dispersive X-ray spectrum, X-ray photoelectron spectroscopy (XPS, ULVAC PHI5000 Versaprobe III, Japan) and optical contact angle measuring instrument (OCA, KRUSS DSA30S, Germany). Nitrogen adsorption/desorption isotherms were measured on an ASAP 2460 physisorption system. The specific surface areas of NiFe precursor/NF and NiFeP@FeOOH/NF were estimated based on the Brunauer–Emmtt–Teller (BET) model.

2. Electrochemical measurement

CHI660E electrochemical workstation equipped with three-electrode configuration was used for electrochemical experiments. In particular, the produced sample (1 cm×1 cm), standard Hg/HgO electrode, platinum sheet and counter electrode were directly used as working electrode (WE), reference electrode and counter electrode respectively. Ahead to the OER test, 20 cycles of cyclic voltammetry (CV) at a scanning speed of 50 mV s⁻¹ were performed. The CV test of OER was conducted at a scanning speed of 1 mV s⁻¹ and its linear sweep voltammetry (LSV) test was set at 5 mV s⁻¹. Electrochemical impedance spectroscopy (EIS) was performed with an amplitude of 5 mV in the appropriate frequency range of 100,000 Hz-0.1 Hz. The CV measurement was used to determine the electrochemical electric double layer capacitance (C_{dl}) at scanning speeds of 5, 10, 20, 40, 80, and 100 mV s⁻¹ in the Faraday-free current range. The stability of the catalyst for 1000 cycles in the range of 0.5 v-0.7 v at a scanning speed of 50 mV s⁻¹ was measured by continuous CV. Observing the change in voltage over an 80-hour period at a constant current density (50 mA cm⁻²) allowed researchers to assess the endurance of the sample. Three electrodes were used to conduct the entire water

breakdown. RuO₂ reference electrode preparation using the drop coating approach was also done for comparison. iR compensation was used to correct all potentials in this work (90%). The potentials in this article were converted to the reversible hydrogen electrode (vs. RHE) according to the Nernst equation: $E_{\text{RHE}} = E_{\text{Hg/HgO}} + 0.059\text{pH} + 0.098$. At a room temperature, each of the aforementioned electrocatalytic tests was conducted.

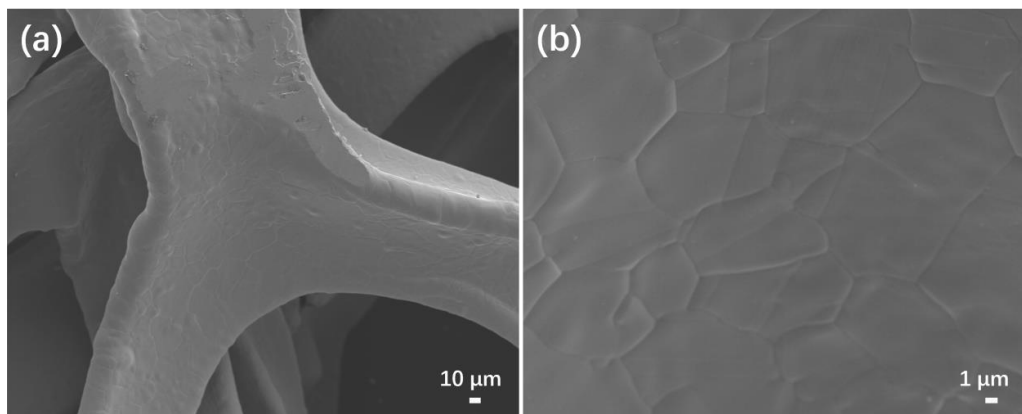


Fig. S1. (a-b) SEM images of NF.

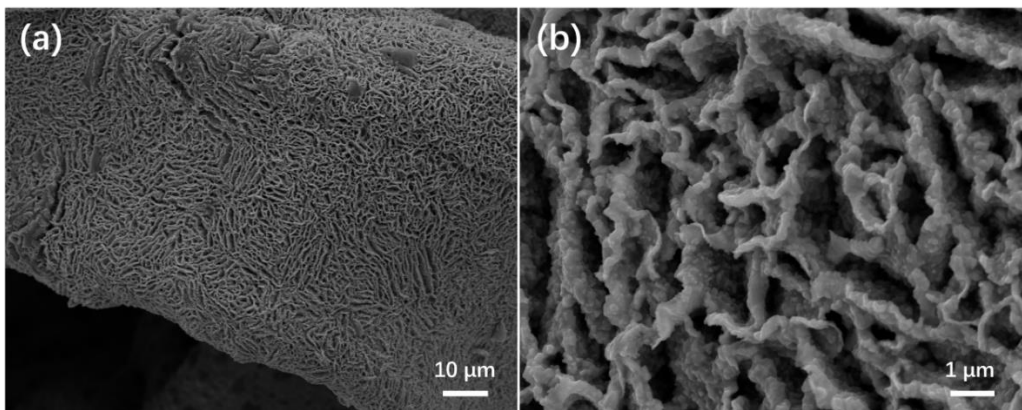


Fig. S2. (a-b) SEM images of Ni₂P/NF.

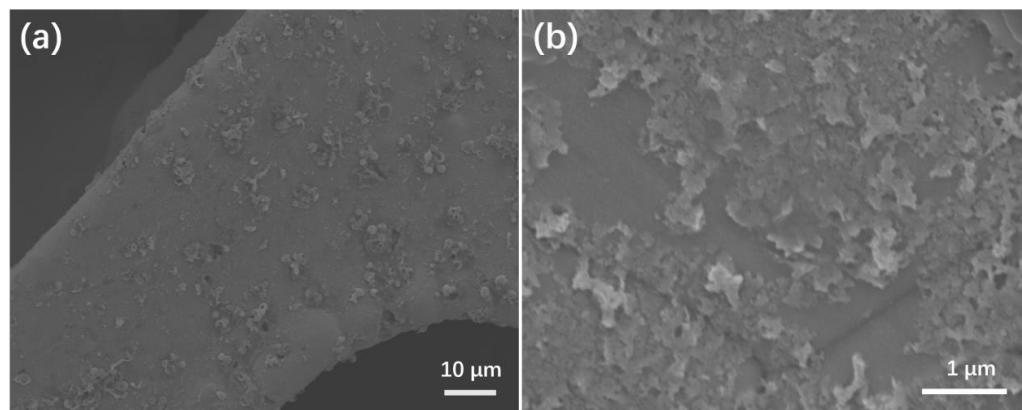


Fig. S3. (a-b) SEM images of FeOOH/NF.

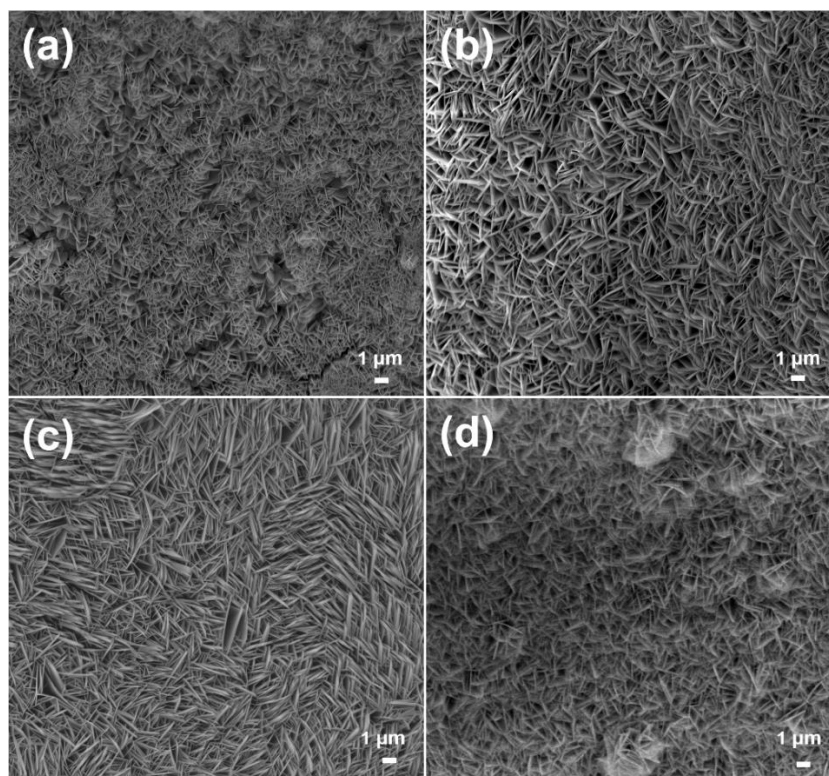


Fig. S4. SEM images of NiFe precursor at different hydrothermal temperatures (a) 50 °C, (b) 100 °C, (c) 120 °C, and (d) 150 °C.

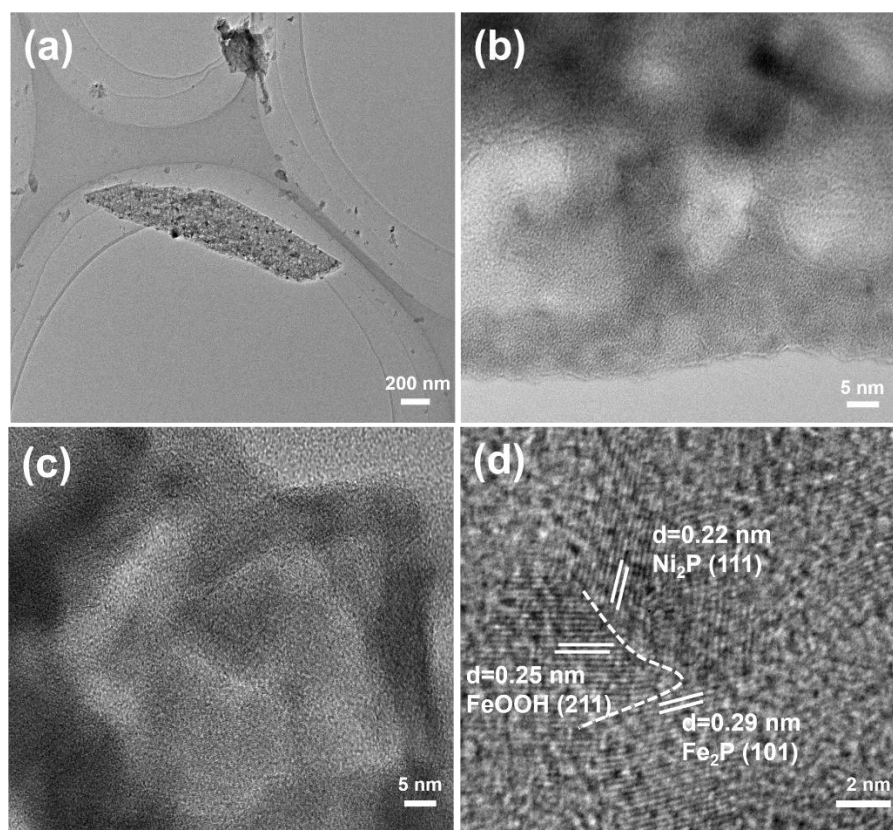


Fig. S5. (a-d) HRTEM images of the NiFeP@FeOOH/NF



Fig. S6. NiFeP@FeOOH/NF contact angle test.

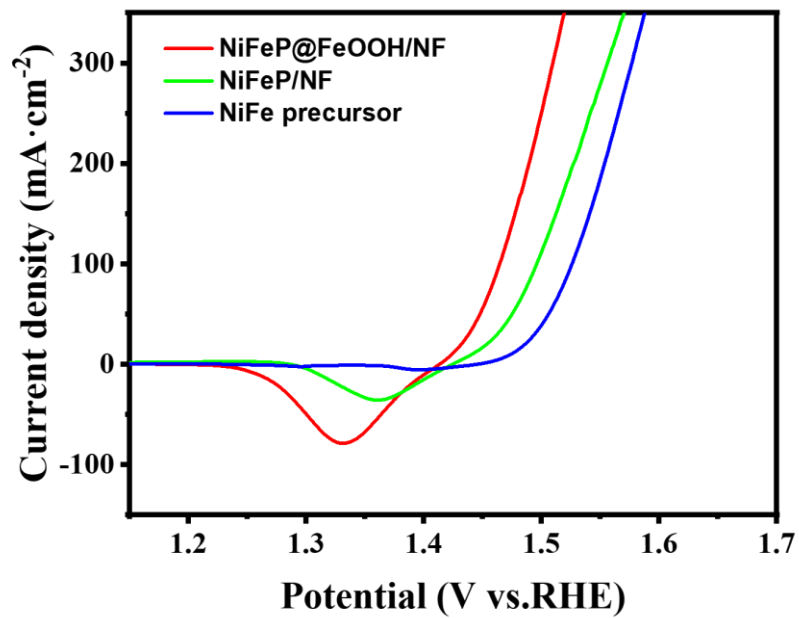


Fig. S7. LSV of NiFe precursor, NiFeP/NF, and NiFeP@FeOOH/NF.

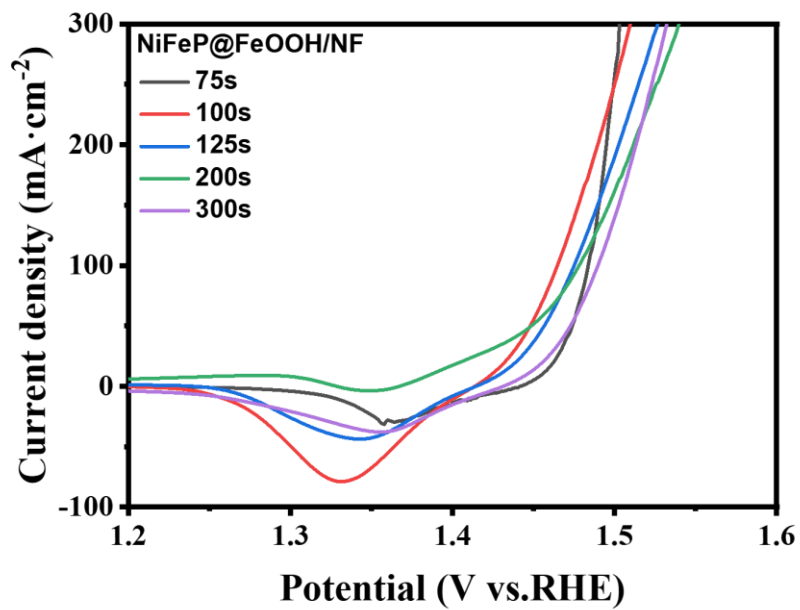


Fig. S8. NiFeP@FeOOH/NF LSV curves of different electrodeposition times.

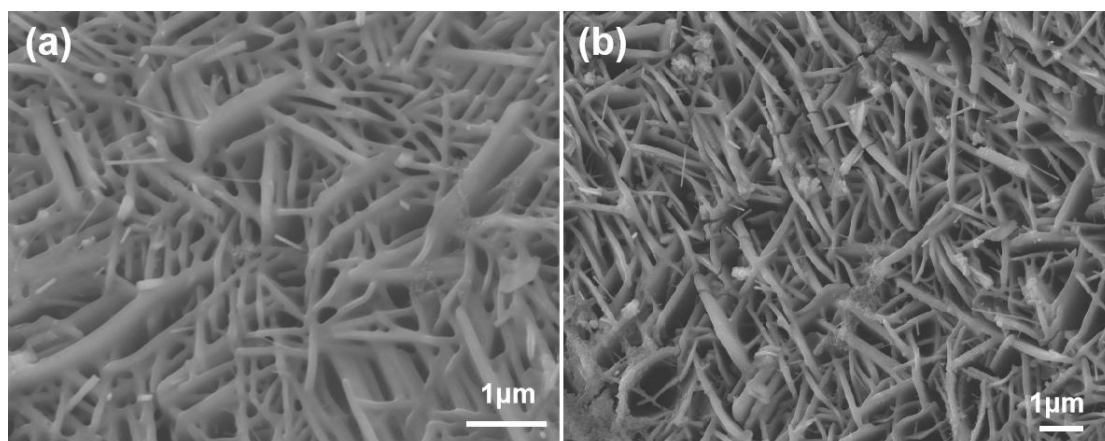


Fig. S9. (a) NiFeP@FeOOH/NF electrodeposition of 125 s, (b) NiFeP@FeOOH/NF electrodeposition of 200 s.

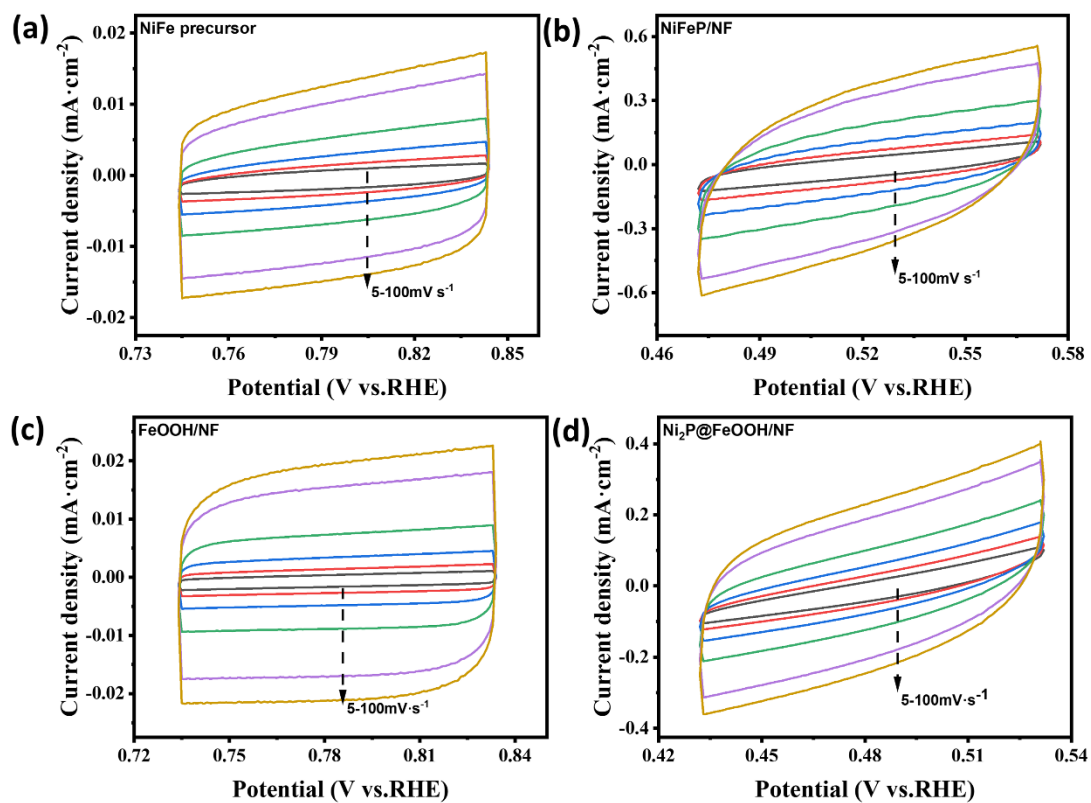


Fig. S10. ECSA was measured by cyclic voltammetry at a scanning speed ranging from 5 mV s⁻¹ to 100 mV s⁻¹ (a) NiFe precursor, (b) NiFeP/NF, (c) FeOOH/NF, and (d) Ni₂P@FeOOH/NF.

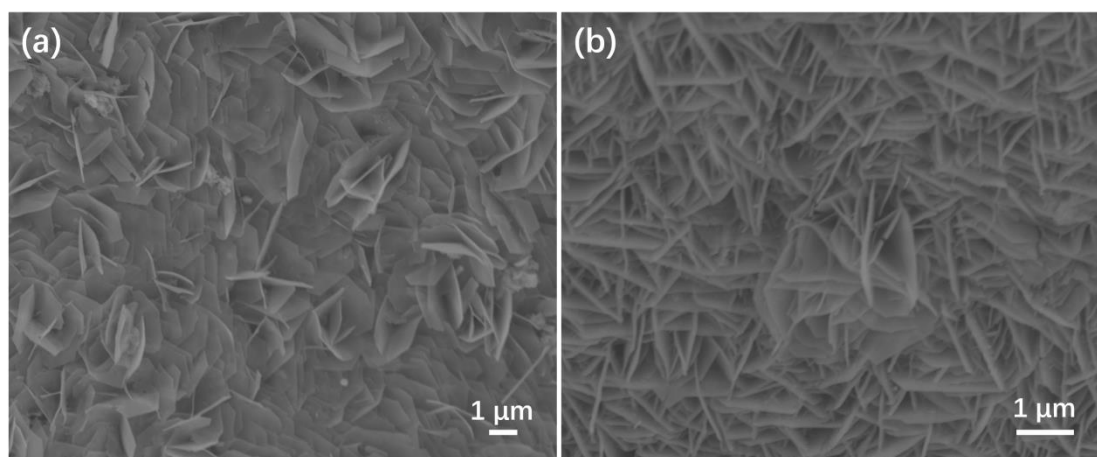


Fig. S11. (a) SEM image after stability test, (b) SEM image after 1000 CV cycle.

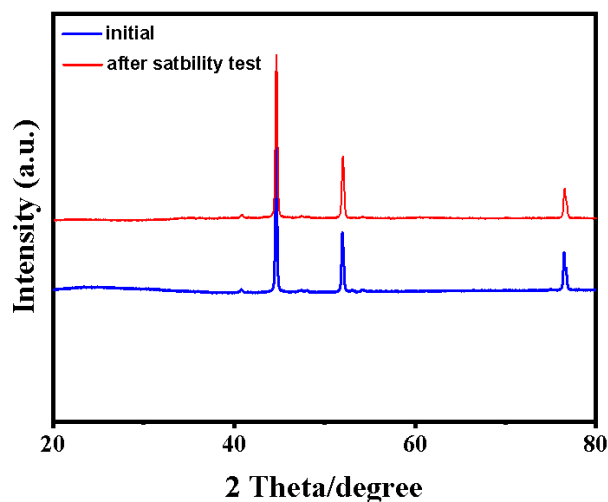


Fig. S12. XRD patterns of NiFeP@FeOOH/NF initial and after stability test high resolution High-resolution fitted.

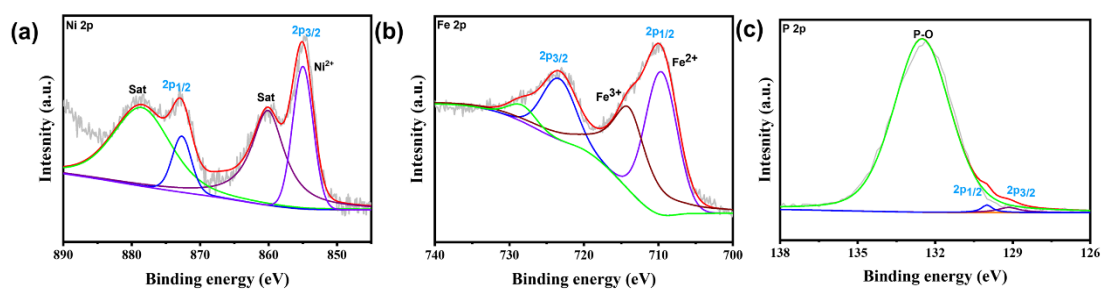


Fig. S13. XPS spectra of NiFeP@FeOOH/NF after stability (a) Ni 2p, (b) Fe 2p, and (c) P 2p.

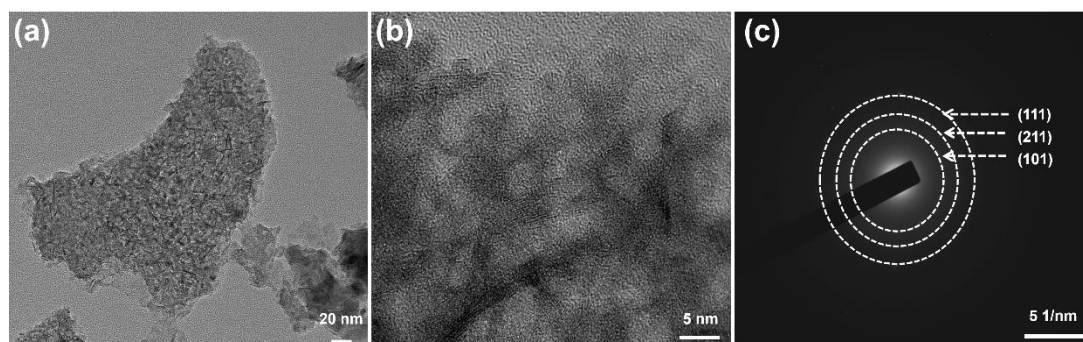


Fig. S14. (a-b) HRTEM images of the NiFeP@FeOOH/NF after 1000 CV cycle, (c) SAED image of NiFeP@FeOOH/NF after 1000 CV cycle.

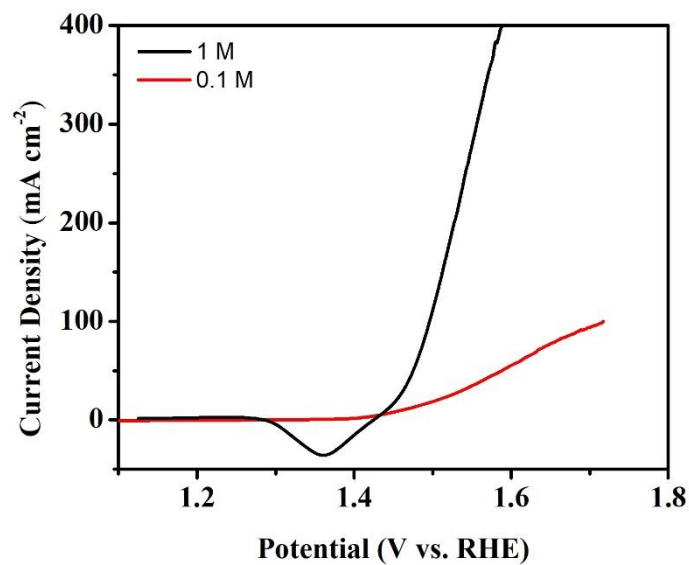


Fig. S15. OER LSV curves of NiFeP@FeOOH/NF in 1.0 M and 0.1 M KOH alkaline solutions.

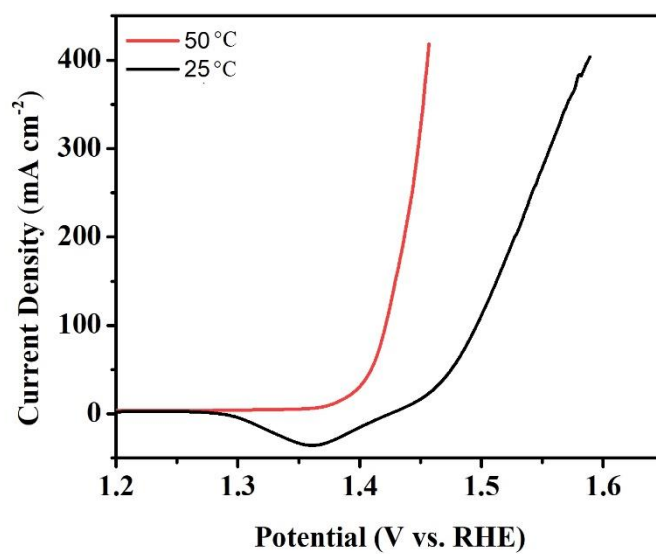


Fig. S16. OER LSV curves of NiFeP@FeOOH/NF at 50 °C and 25 °C in 1.0 M KOH alkaline solution.

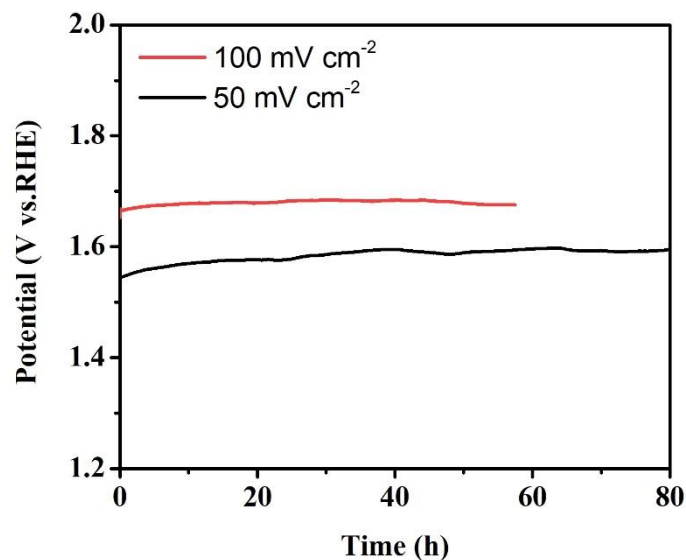


Fig. S17. Long-term durability test of NiFeP@FeOOH/NF at 100 and 50 mA cm⁻² current densities.

Table S1. Comparison of binding energies of NiFeP@FeOOH/NF and NiFeP/NF.

Binding Energy	Ni (eV)			Fe (eV)			P	
	Ni 2p1/2	Ni 2p3/2	Ni-P	Fe 2p1/2	Fe 2p3/2	Fe-P	Fe-P	P-O
NiFeP@FeOOH/NF	874.3	856.3	872.0,	713.1,	710.3,	705.4,	129.7,	133.6
			853.8	728.4	724.1	719.4	130.5	
NiFeP/NF	874.3	856.3	872.0,	713.8,	710.6,	705.4,	129.7,	133.6
			853.8	728.9	724.5	719.4	130.5	

Table S2. Comparison of overpotentials of different OER electrocatalysts at 100 mA cm⁻² in 1.0 M KOH solution.

Electrocatalyst	Overpotential (mV) at 100 mA cm ⁻²	Tafel slope (mV dec ⁻¹)	Reference
NiFeP@FeOOH/NF	235	46.46	This work
MOF-OH/NF	260	77.11	[1]
NiCo ₂ S ₄ /NiFeP/NF	293	110.00	[2]
NiMoO ₄ /NF	253	60.10	[3]

P/NiFe-NiMoO ₄ /NF	300	39.10	[4]
Ni ₂ P/FeOOH	246	62.80	[5]
FeOOH@ β-Ni(Fe)OOH	252	51.49	[6]
NiCo-LDH/NF	303	89.00	[7]
CoFe-LDH/CoFe ₂ O ₄ /NF	400	85.60	[8]
Co-NiSe/NF	380	111.00	[9]
M-NiFe LDH	270	45.10	[10]
Ni-Fe-P/NF	270		[11]
NiOOH@FeOOH	250		[12]
NiFeP@N, C doped carbon cloth	270	47.00	[13]
NiCoP	277	83.00	[14]
Mo-NiCoP	364	60.00	[15]
Ni/NiCoP	345	80.00	[16]
CoFePO	274	51.70	[17]
NiFeP/NF	253	43.70	[18]
Ni-FexP@NF	267	37.00	[19]
NiMoP ₂ nanowires@carbon cloth	260	90.2	[20]

References

- [1] G. Guo, D. Zhong, T. Zhao, G. Liu, J. Li, Q. Zhao, NiCo-BDC derived Co³⁺ enriched NiCo_xO_y/NF nanosheets for oxygen evolution reaction, *Int. J. Hydrogen Energy*. 47

(2022) 23094-23105.

[2] J. Jiang, F. Li, H. Su, Y. Gao, N. Li, L. Ge, Flower-like NiCo₂S₄/NiFeP/NF composite material as an effective electrocatalyst with high overall water splitting performance, *Chin. Chem. Lett.* 33 (2022) 4367-4374.

[3] H. Hao, Y. Li, Y. Wu, Z. Wang, M. Yuan, J. Miao, Z. Lv, L. Xu, B. Wei, In-situ probing the rapid reconstruction of FeOOH-decorated NiMoO₄ nanowires with boosted oxygen evolution activity, *Mater. Today Energy.* 23 (2022) 100887.

[4] S. Zhuang, S. Tong, H. Wang, H. Xiong, Y. Gong, Y. Tang, J. Liu, Y. Chen, P. Wan, The P/NiFe doped NiMoO₄ micro-pillars arrays for highly aereaction towards overall water splitting, *Int. J. Hydrogen Energy.* 44 (2019) 24546-24558.

[5] Y. Zhang, L. You, Q. Liu, Y. Li, T. Li, Z. Xue, G. Li, Interfacial charge transfer in a hierarchical Ni₂P/FeOOH heterojunction facilitates electrocatalytic oxygen evolution, *ACS Appl. Mater. Interfaces.* 13 (2021) 2765-2771.

[6] Y. Li, Y. Wu, M. Yuan, H. Hao, Z. Lv, L. Xu, B. Wei, Operando spectroscopies unveil interfacial FeOOH induced highly reactive β-Ni (Fe) OOH for efficient oxygen evolution, *Appl. Catal. B Environ.* 318 (2022) 121825.

[7] X. Shi, J. Li, X. Zhang, J. Guo, MOF derived NiCo-LDH hollow structure for oxygen evolution reaction, *J. Phys. Chem. Solids.* 172 (2023) 11105.

[8] Z. Guo, X. Wang, F. Yang, Z. Liu, Synergistic effect of Co and Fe bimetallic oxides/hydroxides composite structure as a bifunctional electrocatalyst for enhancing overall water splitting performance, *J. Alloys Compd.* 895 (2022) 162614.

[9] D. Liang, J. Mao, P. Liu, J. Li, J. Yan, W. Song, In-situ doping of Co in nickel selenide nanoflower for robust electrocatalysis towards oxygen evolution, *Int. J. Hydrogen Energy.* 45 (2020) 27047-27055.

[10] Z. Zheng, D. Wu, G. Chen, N. Zhang, H. Wan, X. Liu, R. Ma, Microcrystallization and lattice contraction of NiFe LDHs for enhancing water electrocatalytic oxidation, *Carbon Energy.* 4 (2022) 901-913.

[11] J. Zhang, K. Hou, Q. Yao, C. Wu, M. Huang, L. Guan, Heterogeneous Ni-Fe-P integrated with nickel foam as an efficient and durable electrocatalyst for water oxidation, *Int. J. Hydrogen Energy.* 44 (2019) 11684-11694.

- [12] B. Wu, S. Gong, Y. Lin, T. Li, A. Chen, M. Zhao, L. Chen, A unique NiOOH@FeOOH heteroarchitecture for enhanced oxygen evolution in saline water, *Adv. Mater.* 34 (2022) 2108619.
- [13] J. Bian, Z. Song, X. Li, Y. Zhang, C. Cheng, Nickel iron phosphide ultrathin nanosheets anchored on nitrogen-doped carbon nanoflake arrays as a bifunctional catalyst for efficient overall water splitting, *Nanoscale* 12 (2020) 8443-8452.
- [14] C.G. Read, J.F. Callejas, C.F. Holder, R.E. Schaak, General Strategy for the Synthesis of transition metal phosphide films for electrocatalytic hydrogen and oxygen evolution, *ACS Appl Mater Interfaces* 8 (2016) 12798-12803.
- [15] J. Lin, Y. Yan, C. Li, X. Si, H. Wang, J. Qi, J. Cao, Z. Zhong, W. Fei, J. Feng, Bifunctional electrocatalysts based on Mo-doped NiCoP nanosheet arrays for overall water splitting, *nano-micro letters* 11 (2019) 55.
- [16] Y. Lin, Y. Pan, S. Liu, K. Sun, Y. Cheng, M. Liu, Z. Wang, X. Li, J. Zhang, Construction of multi-dimensional core/shell Ni/NiCoP nano-heterojunction for efficient electrocatalytic water splitting, *Appl. Catal. B Environ.* 259 (2019) 118039.
- [17] J. Duan, S. Chen, A. Vasileff, S.Z. Qiao, Anion and cation modulation in metal compounds for bifunctional overall water splitting, *ACS nano.* 10 (2016) 8738-8745.
- [18] G. Dong, T. Chen, F. Xie, D. Xue, T. Liu, L. Chen, J. Xia, S. Du, F. Wang, F. Xie, J. C. Ho, NiFeP composites supported on Ni foam as an efficient and robust bifunctional electrocatalyst for overall water splitting in alkaline solution, *J. Alloys Compd.* 968 (2023) 171764.
- [19] C. Zhang, Y. Xie, H. Deng, C. Zhang, J.W. Su, Y. Dong, J. Lin, Ternary nickel iron phosphide supported on nickel foam as a high-efficiency electrocatalyst for overall water splitting, *Int. J. Hydrogen Energy.* 43 (2018) 7299-7306.
- [20] X.D. Wang, H.Y. Chen, Y.F. Xu, J.F. Liao, B.X. Chen, H.S. Rao, D.B. Kuang, C.-Y. Su, Self-supported NiMoP₂ nanowires on carbon cloth as an efficient and durable electrocatalyst for overall water splitting, *J. Mater. Chem. A.* 5 (2017) 7191-7199.